# CHAPTER V

# NUMERICAL EXAMPLES

## 5.1. Introduction

The shallow water equations satisfactorily model channel transitions where the bed slope is mild and vertical acceleration is negligible. These transitions include contractions, expansions, bends and embedded bodies, such as bridge piers. These examples are chosen to demonstrate the potential of this design optimization strategy. For circular bends and supercritical flow through contractions, analytic solutions based on restrictive simplifying assumptions are available and are used for comparison purposes with the numerical optimum. For each example, the following information is presented:

1. An analysis of the accuracy of the design space derivatives at one design point.

2. The optimization history showing the efficiency of the optimization algorithm.

3. The water surface profiles for the initial set and the final set of design variables and, when appropriate, the profile for the analytically predicted optimal set of design variables.

4. The shape of the final design, when necessary.

The flow conditions for each example lie in the supercritical regime, so that all flow information is specified at the inlet and no information is specified at the outlet. Furthermore, uniform flow, as given in Appendix E, is used in all the examples to define the velocity profile for the inflow velocity.

The objective function used in these test cases is the variation from average depth over the entire functional domain as given by

$$f(\vec{\beta}) = \sum_{i=n_1}^{n_2} \sum_{j=1}^{NROWS} \left( h_{ave}(\vec{\beta}) - h_{i,j}(\vec{\beta}) \right)^2 \tag{5.1.1}$$

where

$$h_{ave}(\vec{\beta}) = \frac{\sum_{i=n_1}^{n_2} \sum_{j=1}^{NROWS} h_{i,j}(\vec{\beta})}{\sum_{i=n_1}^{n_2} \sum_{j=1}^{NROWS} 1} \tag{5.1.2}$$

For uniform flow, since depth is constant in both directions, this objective function is zero. Thus, the objective function is a measure of the non-uniformity of the flow. The only modification necessary for each example is the specification of the functional domain. Other objective functions can be easily specified by changing the definitions in the appropriate subroutines.

The design space derivatives are estimated via the quasi-analytic formulation of discrete sensitivity analysis, because of the large number of residual functions resulting from the use of the Gauss-Newton method. Highly accurate derivatives are obtained because the Jacobian matrix $\frac{\partial W}{\partial Q}$ is estimated to machine accuracy using the complex Taylor's series expansion method.

With the exception of the straight wall contraction example, which has only one design variable, the Gauss-Newton method is used as the optimization algorithm. The Levenberg-Marquardt constant is defined to be the magnitude of the largest design space derivative for the current design iteration. Thus, the same optimization algorithm is used for all examples with more than one design variable. The design optimization process terminates when the objective function value stabilizes at a single value as measured by the relative change in the objective function, given by equation (3.8.1). As seen in these examples, this choice of termination criterion seems to be quite adequate.

The form of the objective function, the process of estimating the design space derivatives and the optimization algorithm are the same for these examples. The only difference between the examples deal with the grid generation, the inflow conditions and the domain for the objective function. Hence, the design optimization process as applied to these open-channel flow problems appears to be robust and does not require significant modifications in order to be computationally efficient.

## 5.2. Straight Wall Contraction

For channel contractions, a straight wall is often used because only one wave pattern needs to be analyzed. The wall in the contraction makes an angle with the channel walls before and after the contraction. For supercritical flow, this angle along with the Froude number and flow depth, determines the angle of the oblique hydraulic jump that forms at the contraction entrance. When the angle is chosen correctly, the oblique hydraulic jump strikes the opposite wall at the end of the contraction and is

negated by the wave generated at the end of the contraction as shown in Figure 5.2.1. When the optimal contraction length is used, the flow downstream of the contraction is nearly uniform.

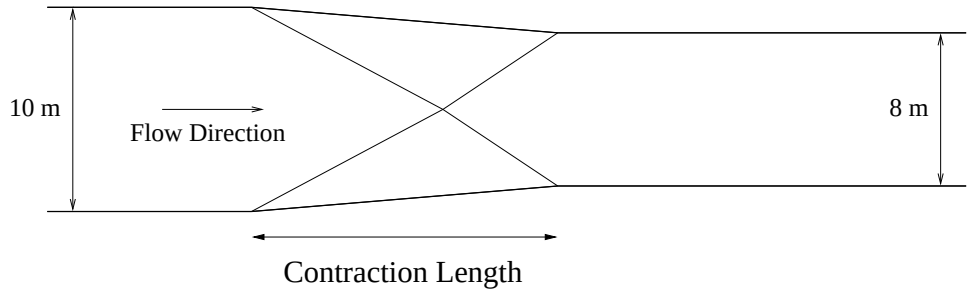


Figure 5.2.1. Wave Pattern Interaction within Contraction.

For a fixed contraction ratio, the contraction length is manipulated so as to approximate this flow pattern. Analytic solutions exist for inviscid flow, and tables created from physical experiments can be used for viscous calculations to determine the optimal contraction length. Unfortunately, the waves generated by the oblique hydraulic jump are smeared as they travel through the contraction, and thus they can not completely be cancelled out at the end of the contraction. As a result, perfectly uniform flow is not achieved.

For this design problem, the contraction length is the only design variable. Thus, the goal is to find the contraction length that generates the flow that is the most uniform. The method of steepest descent with one additional function evaluation is used as the optimization algorithm, because the numerical results indicate that this method was more efficient and stable than the Gauss-Newton method for this one design variable example.

Table 5.2.1. Geometry and Flow Characteristics for Contraction Examples.

| Characteristic | Value |
|---|---|
| Width Before Contraction | 10.0 $m$ |
| Width After Contraction | 8.0 $m$ |
| Bed Slope | 0.02 |
| Manning's n | 0.013 |
| Number of Rows | 15 |
| Number of Columns | Variable |
| Number of Columns in Function | 95 |
| Gravity | 9.817 $m/sec^2$ |
| Inflow Depth | 1.5 $m$ |
| Ave. Inflow Velocity | 12.6225 $m/sec$ |
| Ave. Inflow Froude Number | 3.2894 |
| Total Discharge Q | 189.3378 $m^3/sec$ |

The width of the channel contracts from 10.0 m to 8.0 m. The other characteristics of the flow and geometry are listed in Table 5.2.1. The initial contraction length is 15.0 m. The design space derivative as determined via discrete sensitivity analysis for this contraction length is -2.1847708562457. The exact derivative as determined via the complex Taylor's series expansion method applied to the objective function is -2.185030387396. Thus, for the initial design variable, the design space derivative is accurate to four significant digits.

For this example, the design process terminates when the relative change in the objective function is less than $10^{-6}$, which occurs after 9 design iterations. The optimal contraction length is approximately 27.076 m. The optimization history is given in Figure 5.2.2. After 5 iterations, the change in the function value is insignificant.

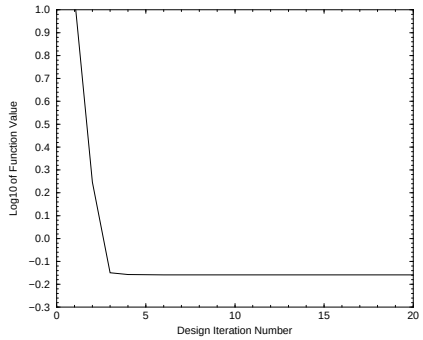


Figure 5.2.2. Optimization History for Straight Wall Contraction.

The depth profiles for the initial contraction length of 15.0 m and the final length of 27.076 m are plotted in Figure 5.2.3. For the sub-optimal contraction length, the flow depths continue to oscillate far downstream of the contraction, requiring higher channel walls for a longer distance of the channel. Furthermore, the water depths within the contraction are much larger. For the optimal contraction length, the oscillations in the downstream flow are much smaller, although they are still present. For the initial contraction length, the maximum depth along the wall in the region downstream of the contraction is approximately 2.1 m; whereas for the final contraction length, the maximum depth is approximately 1.95 m, which reduces the required channel wall height and the cost of building the channel.

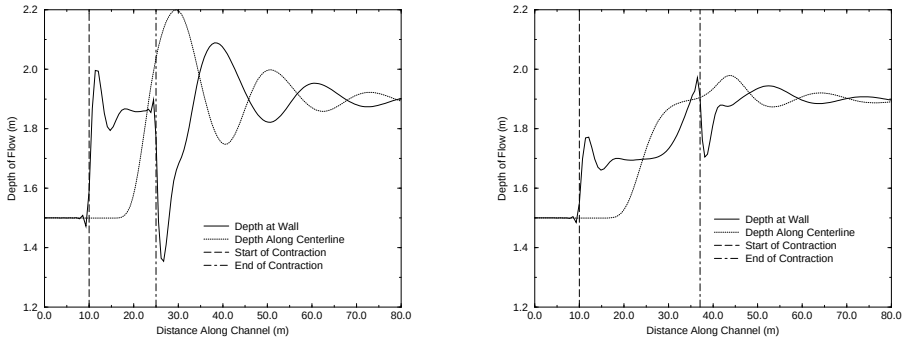


Figure 5.2.3. Water Surface Profiles for Initial and Final Contraction Lengths.

The depths for the entire flow field are plotted in Figure 5.2.4 and show that the wave generated at the beginning of the contraction strikes the opposite wall in the vicinity of the end of the contraction, but the wave is not totally absorbed and continues to reflect downstream. One possible explanation for the lack of wave cancelation is that frictional effects may cause the wave to smear. As a result, the smeared wave will strike a region of the wall rather than exactly at the end of the contraction.

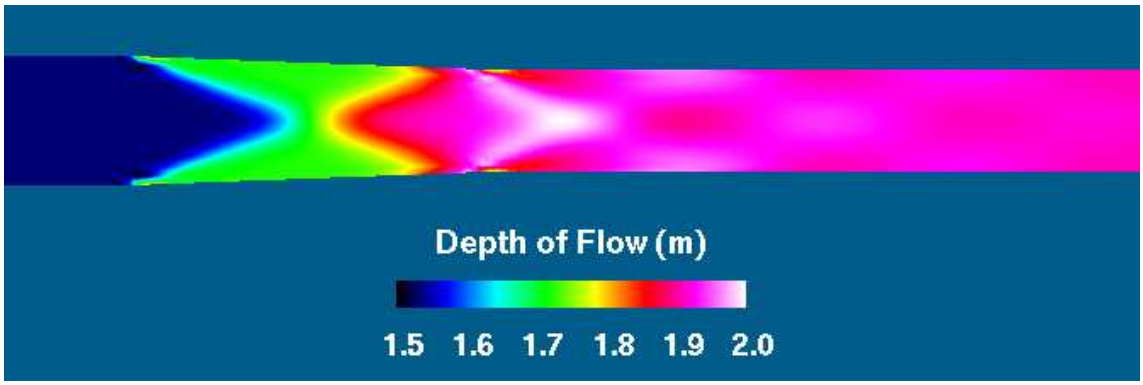


Figure 5.2.4. Depths for the Flow Field for the Final Contraction Length.

Using the analytic methods arising from inviscid, oblique hydraulic jump equations, the optimal contraction length is 25.053 m, which is approximately 7.5% shorter than the numerical result. The analytic methods make more simplifying assumptions than the shallow water equations, including the assumption of a uniform velocity distribution, parallel streamlines and inviscid flow. Since HIVEL2D does not make these assumptions, the optimal contraction length predicted by HIVEL2D is different from the analytic result and is probably closer to the physical optimum. Using the analytic result for the contraction length, the flow produced by HIVEL2D is slightly less uniform than the numerically determined optimum. The depth profile for the analytic result is plotted in Figure 5.2.5. The contraction length found by using the analytic methods produces a flow field that is quite similar to the flow field for the optimal contraction length.

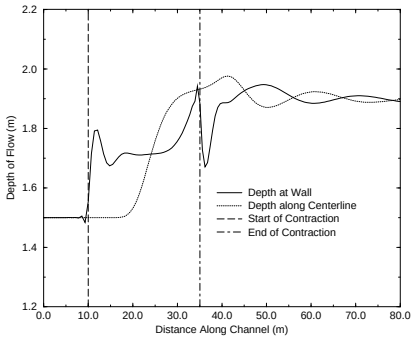


Figure 5.2.5. Water Surface Profiles for Analytically Determined Length.

In Figure 5.2.6, the objective function is graphed versus contraction length, which shows that the objective function does not change significantly over a large range of design variables. Contraction lengths within this range probably perform in similar fashions. Thus, because the waves generated by the oblique hydraulic jumps are

not totally absorbed at the end of the contraction, there appears to be wide range of contraction lengths that demonstrate similar performance. Actually, Figure 5.2.6 indicates that any length over approximately 23 m will produce similar results.

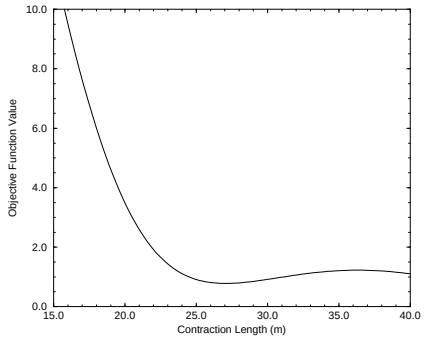


Figure 5.2.6. Function Value versus Length for Straight Wall Contraction.

For the straight wall contraction example, the design optimization process uses design space derivatives that are accurate to four significant digits to drive the contraction length to the optimal length within 9 design iterations. The optimal contraction length, as identified by the design process, is similar to the analytic, inviscid result, and produces a slightly more uniform flow than the analytic result. Unfortunately, because the waves within the contraction are not totally absorbed at the end of the contraction, perfectly uniform flow is not achieved using a straight wall contraction.

## 5.3. Curved Wall Contraction

In the design of channel contractions, there may not be enough land to build a straight wall contraction with optimal length due to other existing structures. In these cases, a curved wall can be used in a contraction whose length is sub-optimal for a straight wall contraction. By using a curved wall, multiple wave patterns are generated and interact in a complicated fashion. By designing the curve properly,

the resulting wave patterns can be made to cancel each other out, generating uniform flow almost immediately downstream of the contraction. In this example, the design optimization process satisfactorily identifies an excellent curve for a sub-optimal contraction length using 9 design variables. The resulting channel generates a set of waves that cancel out almost exactly, producing downstream flow that is nearly uniform.

For this example, the channel contraction of the previous section is used with the exception that the contraction length is fixed at 17.5 m. Thus, the length is much shorter than optimal for a straight wall contraction for this flow. The shape of the curved wall is defined by a B-spline curve with thirteen control points. The middle nine control points are used as the design variables, and the outer control points are fixed to ensure smooth connections with the channel. The initial design variables are chosen to mimic a straight wall contraction.

Table 5.3.1. Comparison of Design Space Derivatives for Curved Wall Contraction.

| Design Variable | Discrete Sensitivity Analysis | Complex Expansion Method |
|---|---|---|
| 1 | -20.230174451859 | -20.230174307571 |
| 2 | -36.748576544393 | -36.748575877468 |
| 3 | -41.216698900486 | -41.216699449246 |
| 4 | -39.130277285368 | -39.130276821952 |
| 5 | -30.501233478923 | -30.501234074469 |
| 6 | -16.901359973716 | -16.901359500428 |
| 7 | -0.41986147376448 | -0.41986098877364 |
| 8 | 15.503612229261 | 15.503610968565 |
| 9 | 7.7905147152597 | 7.7905144427567 |

For the initial set of design variables, the design space gradients as approximated via discrete sensitivity analysis and complex Taylor's series expansions are calculated

and presented in Table 5.3.1. These derivatives agree to a least six significant digits.

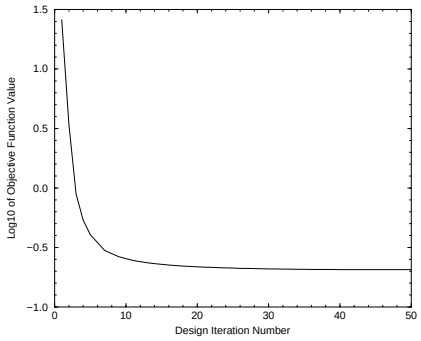


Figure 5.3.1. Optimization History for Curved Wall Contraction.

The design optimization process terminates when the change in the objective function value is less than $10^{-5}$, which occurs after 33 iterations. The optimization history is plotted in Figure 5.3.1 and shows that the function value decreases rapidly within the first ten iterations, decreases much more slowly after ten iterations and continues to decrease slightly after 30 iterations. The primary reason for this failure is that the derivative for the first design variable does not converge to zero but remains relatively large. This derivative is negative, indicating that the first design variable should be larger. The optimal contraction curve, shown in Figure 5.3.2, makes a sharp angle with the channel initially, producing a strong oblique hydraulic jump.

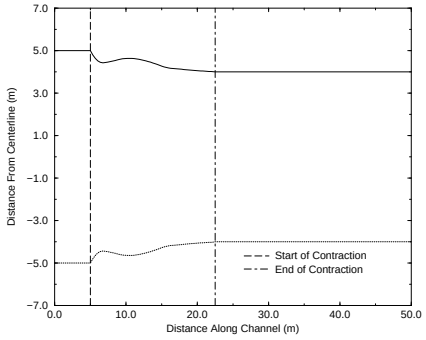


Figure 5.3.2. Shape of Optimal Wall for Curved Wall Contraction.

The water surface profiles for the initial straight wall contraction and the optimal curved wall contraction are plotted in Figure 5.3.3. The depths for the straight wall contraction continue to oscillate downstream of the contraction. For the optimal curved wall contraction, the depths are almost uniform immediately after the contraction. At the beginning of the contraction, the depth spikes to about 5.0 m in the numerical simulation, resulting from the sharp turn that the wall makes into the flow. Special care is needed to analyze the physical significance of these spikes as the shallow water equations, which do not model vertical motion, are violated in this vicinity. Another observation from the plots in Figure 5.3.3 is that the depth along the wall for the final design is approximately the same as the maximum depth along the wall for the initial design. Even though the wave patterns have been removed, the height of the channel walls will need to be at least as high for the final design as for the initial design. These failures, though, are not the results of the design optimization process but rather are caused by the limitations of the shallow water equations and by the choice of objective function. Actually, the design optimization process was successful in determining a design that produced a flow with uniform depth immediately downstream of the contraction. By using a numerical model that includes vertical effects and by developing a more appropriate objective function, the design optimization process may be more successful in identifying a solution whose wall heights are smaller.

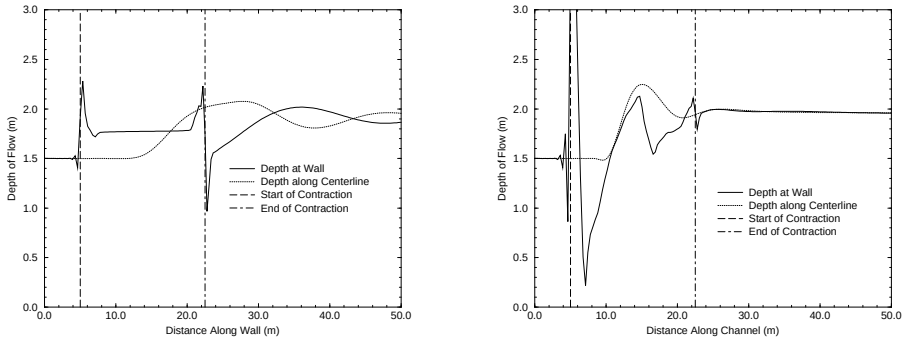


Figure 5.3.3. Flow for Initial and Final Design for Curved Wall Contraction.

Finally, the flow depths for the entire flow field through the optimal curve is given in Figure 5.3.4. As shown in this plot, multiple waves are generated by the curved wall contraction, and these waves negate each other almost immediately downstream of the contraction.

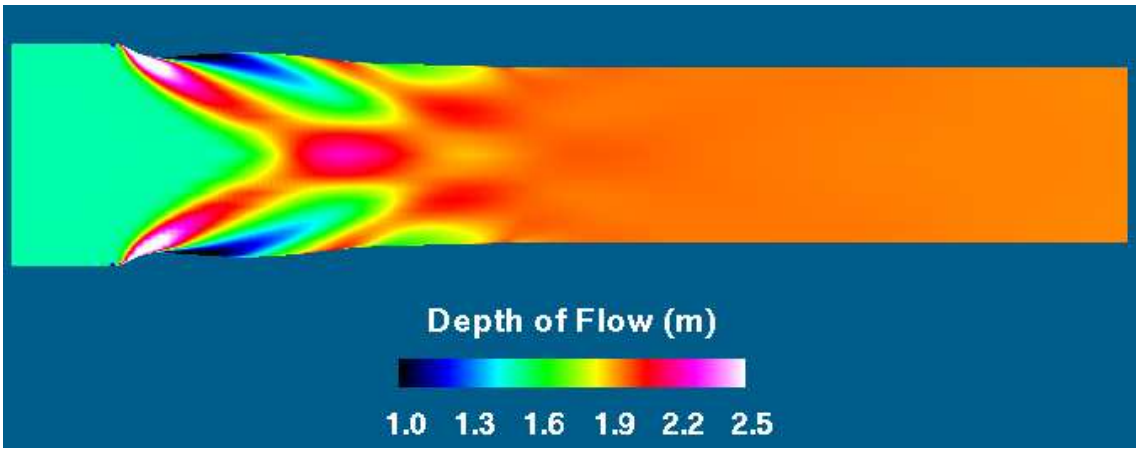


Figure 5.3.4. Depths for the Flow Field for Optimal Curved Wall Contraction.

As seen in this example, the numerical design optimization process is able to identify a region of the design space that produces flow that is nearly uniform. Without any knowledge about the behavior of oblique hydraulic jumps and smearing of

the resulting waves, the design process is able to manipulate these waves so as to negate one another and achieve the design objective.

## 5.4. Curved Wall Expansion

Channel expansions are the opposite of channel contractions in many ways beyond their shapes. At the beginning of an expansion, the wall turns away from the flow which produces a drop in the water level, and a negative wave is formed. If the expansion consists of a straight wall, the expansion length can be manipulated so that this negative wave strikes the opposite wall at the end of the expansion and is negated, just as in a channel contraction. In contractions, a designer needs to avoid choked flow, which results when the specific discharge $q$ becomes too large for the specific energy as shown in Figure 5.4.1. Assuming that the channel flow has a specific energy of $E_o$ and a discharge of $q_2$ before the contraction and that energy losses are negligible, if the discharge after the contraction is $q_3$, then choked flow will not be formed because the curve for $q_3$ intersects the specific energy line $E_o$. However, if the channel contracts so that the discharge becomes $q_4$, choked flow will occur because the curve for $q_4$ does not intersect the specific energy line.

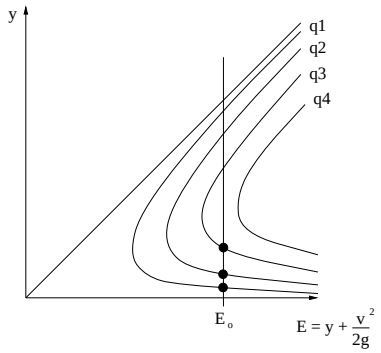


Figure 5.4.1. Specific Energy Diagram for Contractions and Expansions.

In an expansion, the specific discharge decreases, which implies that choked flow is not possible. However, for supercritical flow, as the specific discharge drops, the velocity will increase as will frictional losses. If the frictional slope $S_f$ becomes larger than the bed slope $S_o$, then the depth of the flow will increase as given by

$$\frac{dh}{dx} = \frac{S_f - S_o}{Fr^2 - 1} \tag{5.4.1}$$

where $Fr$ is the Froude number. If $S_f$ increases enough so that normal depth ($S_f = S_o$) is larger than critical depth ($Fr = 1$), then the flow depth will increase until it reaches critical depth, where it will transition from supercritical to subcritical flow via a hydraulic jump. As a result, the designer of an expansion must avoid a channel that expands too much, just as a contraction designer must avoid a channel that contracts too much. These difficulties are primarily governed by the amount of contraction or expansion and not by the shape of the channel. Thus, this numerical design optimization process can not be used to overcome these restrictions.

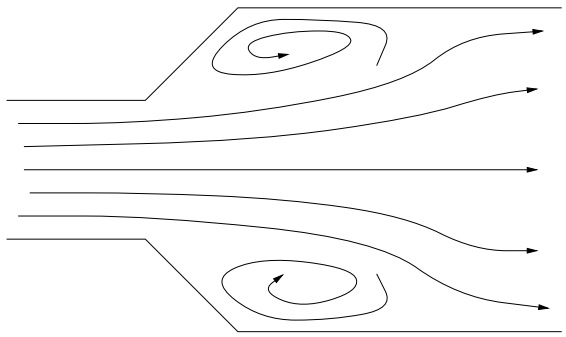

Figure 5.4.2. Separation and Recirculation in Channel Expansions.

Finally, in a contraction, if the wall turns into the flow too sharply, the water will splash against the wall and may over top the wall or cause other unexpected and

undesirable events. Similarly, in an expansion, if the wall turns away from the flow too rapidly, separation and recirculation of flow may occur, as shown in Figure 5.4.2. This highly turbulent flow is difficult to model accurately, can cause unexpected flow patterns, and should be avoided in the design process.

Table 5.4.1. Geometry and Flow Characteristics for Expansion.

| Characteristic | Value |
|---|---|
| Width Before Expansion | 8.0 $m$ |
| Width After Expansion | 10.0 $m$ |
| Bed Slope | 0.02 |
| Manning's n | 0.013 |
| Number of Rows | 25 |
| Number of Columns | variable |
| Number of Columns in Function | 95 |
| Gravity | 9.817 $m/sec^2$ |
| Inflow Depth | 1.5 $m$ |
| Ave. Inflow Velocity | 12.273 $m/sec$ |
| Ave. Inflow Froude Number | 3.198 |
| Total Discharge Q | 147.27 $m^3/sec$ |

For this design optimization example, the optimum length for a straight wall expansion is determined. Using this length, a nine design variable curved wall expansion is generated with the goal of producing uniform downstream flow. Thus, this example presents some of the difficulties of designing channel expansions and highlights the ability of curved wall expansions to generate highly uniform flow.

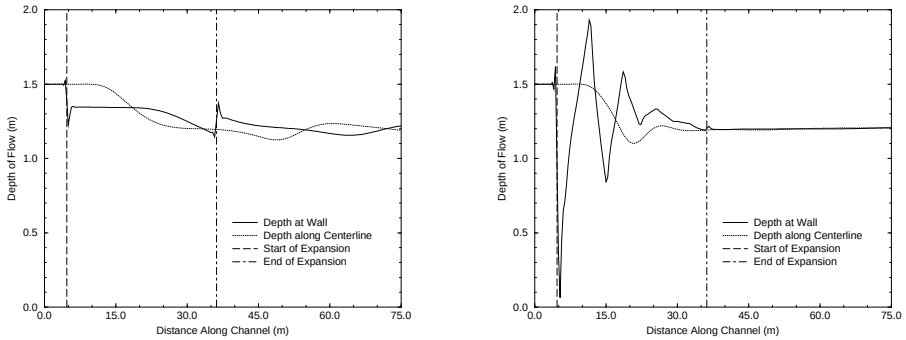


Figure 5.4.3. Water Surface Profiles for Straight and Curved Wall Expansions.

The channel and inflow characteristics are given in Table 5.4.1. The channel expands from 8 m to 10 m. By applying the design optimization process to a straight wall expansion with these characteristics, the optimal expansion length is determined to be approximately 31.5 m. The water surface profile for this straight wall expansion is plotted in Figure 5.4.3. Using this length and a curved side wall for the expansion, the design optimization process is able to find an expansion curve that generates nearly uniform downstream flow as shown in Figure 5.4.3. To be able to generate this flow, the depth of flow within the expansion varies greatly. Since the shallow water equations ignore vertical motion, which is clearly necessary in some regions of the flow, these spikes and dips may not be physically accurate, requiring the need for scale models to ascertain the physically realistic flow field.

Table 5.4.2. Comparison of Design Space Derivatives for Expansion.

| Design Variable | Discrete Sensitivity Analysis | Complex Expansion Method |
|---|---|---|
| 1 | -6.3191267345463 | -6.3191266430156 |
| 2 | -9.4086058618832 | -9.4086057425225 |
| 3 | -4.5262903680480 | -4.5262904226085 |
| 4 | 2.4959126969699 | 2.4959125439619 |
| 5 | 8.5079222789518 | 8.5079223727074 |
| 6 | 12.529373549894 | 12.529373713910 |
| 7 | 12.733065392482 | 12.733065441961 |
| 8 | 7.3833227827076 | 7.3833228013653 |
| 9 | -1.3538957675103 | -1.3538957769861 |

In order to validate the accuracy of the design space derivatives, these derivatives are compared with the results from the complex Taylor's series expansion method for the initial set of design variables, which mimics the straight wall contraction. These results are presented in Table 5.4.2 and indicate that each of these derivatives agree with the more accurate complex expansion method to at least seven significant digits.

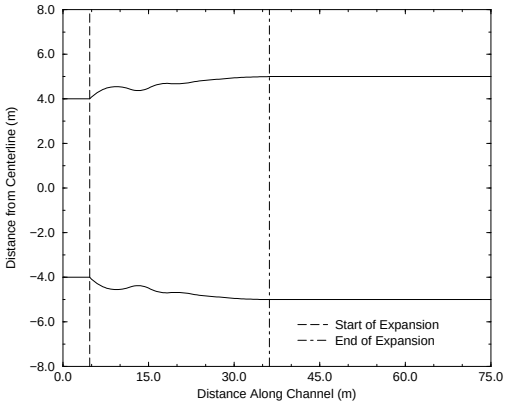


Figure 5.4.4. Optimum Shape for Curved Wall Expansion.

To achieve uniform downstream flow, the expansion initially turns away from the flow as shown in Figure 5.4.4. Eventually, the design process generates a curve that turns away from the flow so rapidly that the water depth along the wall is zero. As

a result, the flow solver fails, and the design process terminates. The optimization history is graphed in Figure 5.4.5, which shows that most of the design improvement occurs within the first five iterations. Thus, the design optimization process can be terminated many design iterations before these numerical difficulties occur.

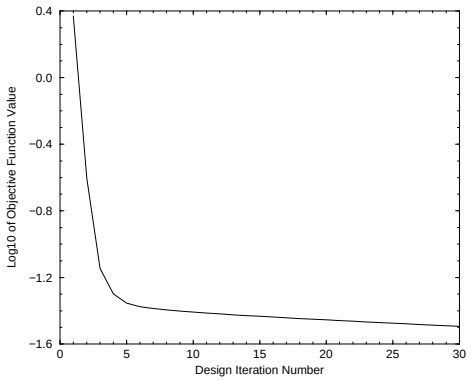


Figure 5.4.5. Optimization History for Curved Wall Expansion.

Finally, the depths throughout the straight wall expansion and curved wall expansion are pictured in Figure 5.4.6. Using the design optimization process, the optimal straight wall expansion length is determined, and using this length, a curved wall expansion is designed which produces nearly uniform flow, unlike the straight wall expansion. Thus, curved walls can be used to generate waves that cancel each other. Furthermore, this example demonstrates that the numerical design process is a tool that needs to be used in conjunction with scale models and other techniques, in order to ensure a successful design.

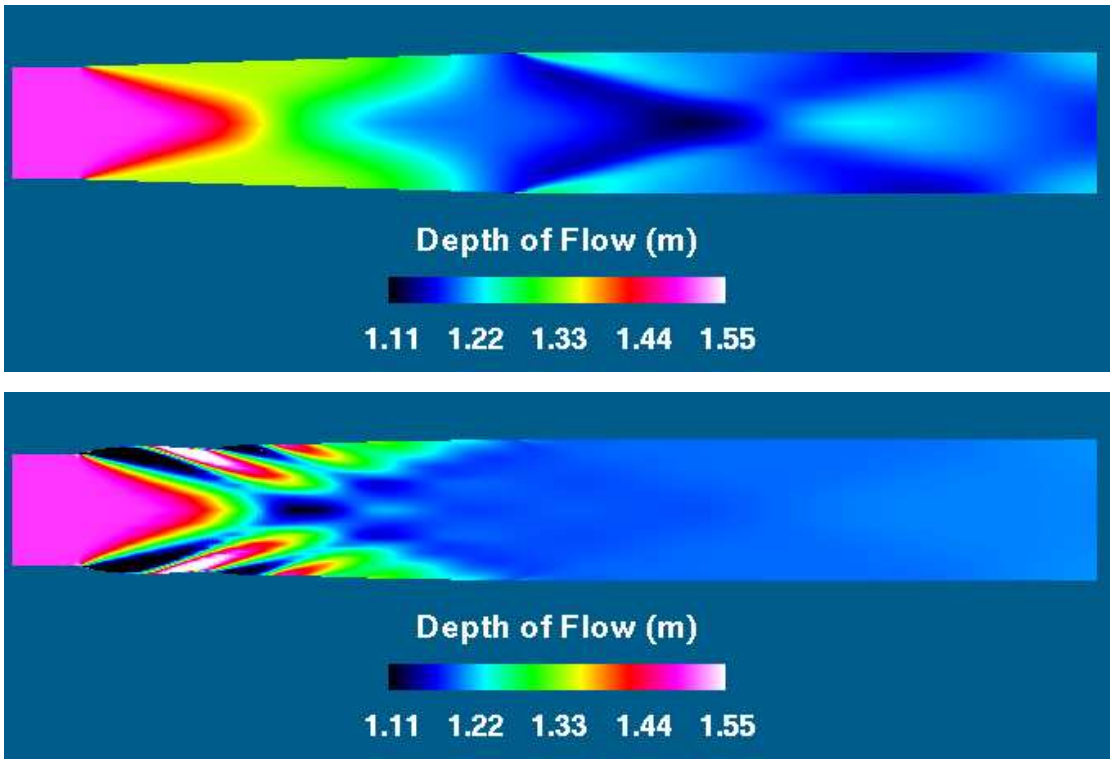


Figure 5.4.6. Depths for the Flow Field for Straight and Curved Wall Expansions.

## 5.5. Circular Channel Bend

Another type of channel transition that can be modeled via the shallow water equations is the circular bend. Typically, the bed in a bend is sloped across the channel to provide a force which balances the centripetal force of the fluid through the bend. By analyzing these forces, analytic results for the transverse bed slope can be derived. Before and after the bend, there is no transverse bed slope. Thus, the transition from the region of no bed slope to the region within the bend must be analyzed carefully; otherwise, waves can be generated within the bend because of these transitions regardless of the amount of transverse bed slope. For this example, 50 design variables define a B-spline curve for the amount of transverse bed slope

before, during and after the bend. Furthermore, the domain of the objective function includes the regions before and within the bend, as well as the region after the bend.

Table 5.5.1. Geometry and Flow Characteristics for Circular Channel Bend.

| Characteristic | Value |
|---|---|
| Channel Width | 10.0 $m$ |
| Bed Slope | 0.012 |
| Manning's n | 0.013 |
| Inner Radius of Bend | 100.0 $m$ |
| Number of Rows | 21 |
| Number of Columns | 380 |
| Number of Columns in Function | 370 |
| Gravity | 9.817 $m/sec^2$ |
| Inflow Depth | 0.7 $m$ |
| Ave. Inflow Velocity | 6.2563 $m/sec$ |
| Ave. Inflow Froude Number | 2.387 |
| Discharge Q | 43.794 $m^3/sec$ |

The characteristics of this example are given in Table 5.5.1, and the channel is graphed in Figure 5.5.1. The channel makes a $90^o$ bend through a radius of curvature of 105.0 m along its centerline. Of the 380 columns of nodes, 370 are included in the objective function. Given these flow and geometry parameters, an analytically predicted transverse bed slope of 0.0380 is needed to balance the bed slope forces and centripetal forces. This analytic result is based on assumptions that the velocity distribution is uniform across the channel and that the radius of curvature for the entire flow is 105.0 m, whereas it actually varies from 100.0 m to 110.0 m across the bend and a non-constant velocity distribution is used.

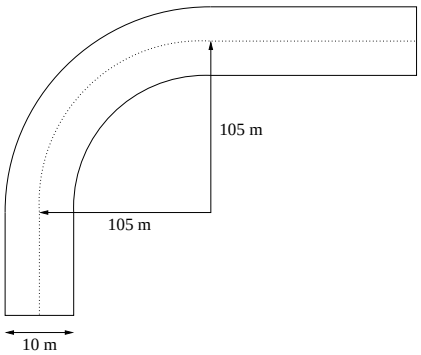


Figure 5.5.1. Geometry for Circular Channel Bend.

The design optimization process starts with a constant transverse bed slope of 0.02 and linear transitions before and after the contraction. Since there are 50 design variables, only a small set of design space derivatives have been analyzed for accuracy. These results are given in Table 5.5.2. These derivatives are in agreement to between six and eight significant digits.

Table 5.5.2 Comparison of Design Space Derivatives for Circular Channel Bend.

| Design Variable | Discrete Sensitivity Analysis | Complex Expansion Method |
|---|---|---|
| 1 | 19.964851067446 | 19.964852378709 |
| 2 | 25.108134826382 | 25.108134714268 |
| 3 | 19.358701999683 | 19.358691597705 |
| 10 | -12.677576340546 | -12.677577631453 |
| 18 | -32.637833170140 | -32.637829687631 |
| 25 | 16.151752162457 | 16.151750639481 |
| 33 | -18.134686276300 | -18.134684699045 |
| 40 | -5.0942054245774 | -5.0942074466819 |
| 47 | -5.3103160489289 | -5.3103194084512 |
| 50 | 0.37009624729716 | 0.37009561184092 |

The design optimization process terminates when the change in the relative objective function value is less than $10^{-6}$; thus, the process terminates after six design iterations, after having found the optimal curve for the transverse bed slope. The optimization history is plotted in Figure 5.5.2 and shows that the objective function converges to its optimum quite rapidly. One reason for the success of the design optimization process is that the value of the bed slope through the curve is relatively constant. Thus this region of the curve can probably be successfully analyzed using fewer control points. Also, since there are no hydraulic jumps in the flow field, the assumption in the shallow water equations concerning the vertical accelerations is not violated, and the numerical design result is probably more reliable.

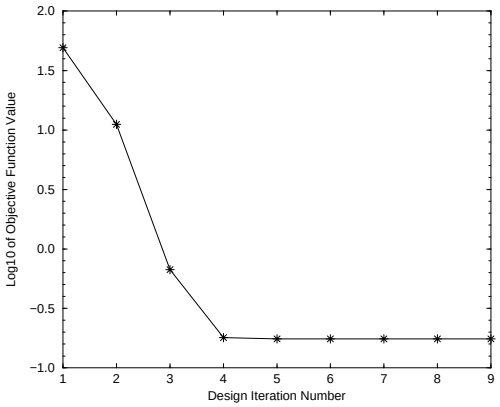


Figure 5.5.2. Optimization History for Circular Channel Bend.

In Figure 5.5.3, the bed and water surface profiles for the optimal solution are plotted along the inner and outer walls and along the centerline. The transverse bed slope for the interior of the circular bend is approximately 0.0398 which is slightly larger than the analytically predicted value of 0.0380. More importantly, though, the optimal transverse bed slope in the regions of bed slope transition are obtained.

These transitions are not linear, but rather the channel bed has one small undulation before the channel bend is reached.

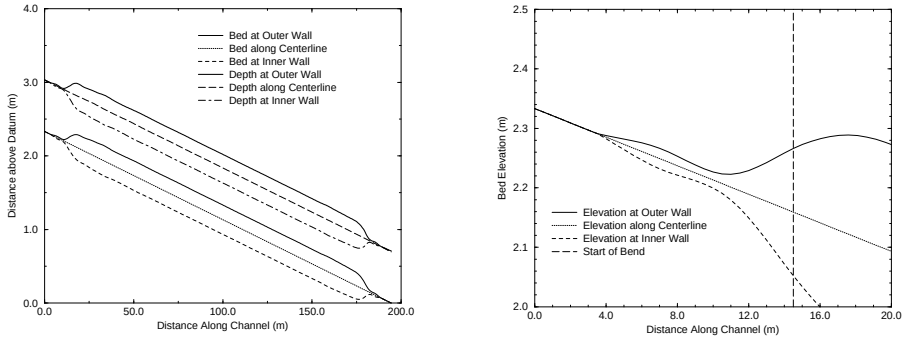


Figure 5.5.3. Bed and Water Surface Profiles for Optimal Circular Channel Bend.

To compare the optimal numerical transverse bed slope with the analytically predicted value, the approach slopes for the numerical optimum are used with the analytically predicted slope. The water surface profiles for the numerical optimum and for the analytic value are given in Figure 5.5.4. In the figure to the left, the water surface profiles for the analytically predicted slope shows that a set of small waves reflects back and forth down the channel, which is not the case for the numerical optimum.

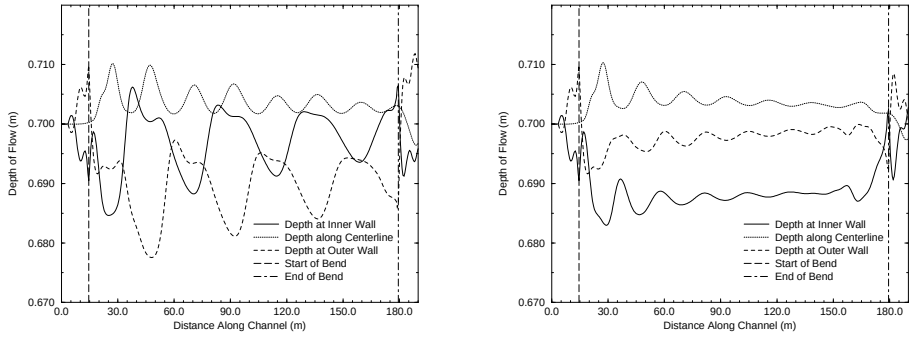


Figure 5.5.4. Water Surface Profiles for Analytical and Numerical Optima.

Finally, the overview of the depths for the optimal solution is plotted in Figure 5.5.5. Even though the water levels are not perfectly uniform throughout the bend, the water travels around the bend without slapping against the walls, resulting in a flow pattern that will not over-top the walls. The waves generated before and after the channel bend result from the transverse bed slopes in these regions. In addition to controlling the transverse bed slope through the bend, the design variables control the slope before and after the bend, so that the channel can prepare the water for the bend and receive it after the bend.


Figure 5.5.5. Depths for the Flow Field for Optimal Circular Channel Bend.

In this example, a sloped bed is used to generate a gravitational force to balance the centrifugal forces in a circular channel bend. The design optimization process is able to generate highly accurate design space derivatives and is able to find the optimal curve quite efficiently, even though the number of design variables is quite

large. Because the water in the channel does not form any hydraulic jumps, the vertical velocity assumption of the shallow water equations are not violated, which suggests that the flow field is physically realistic. The resulting transverse bed slope through the bend is quite similar to the analytic value, and the design process is able to identify the appropriate bed slopes for the approach and exit regions to the bend.

5.6. Embedded Bodies

Bridge piers are a common type of embedded body for open-channels. When a bridge crosses an channel, the designer can either have the channel contract before the bridge and expand after it as in Figure 5.6.1.a so as to avoid the use of bridge piers or can place piers into the flow field as in Figure 5.6.1.b. In either case, the effective channel width decreases, and the discharge rate increases, thus choked flow is an issue that must be addressed.

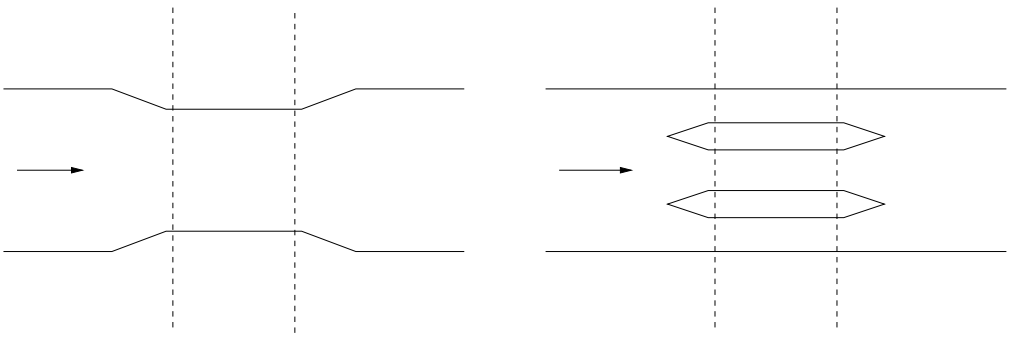

Figure 5.6.1.a Figure 5.6.1.b

Figure 5.6.1. Examples of Bridge Crossings.

Furthermore, the formation of oblique hydraulic jumps near the upstream side of the bridge can cause water to over-top the bridge. To optimize the flow under

the bridge, uniform supercritical flow is again desirable because the maximum water level for the specified energy and discharge is lowest. To achieve uniform flow under the bridge, the piers can be extended upstream of the bridge, and the shape can be modified in this region as in a contraction so that the wave patterns cancel out as the water flows under the bridge. The general shape of one such channel is given in Figure 5.6.2. The shapes of the contraction and of the expansion are controlled by two B-spline curves using six design variable each.

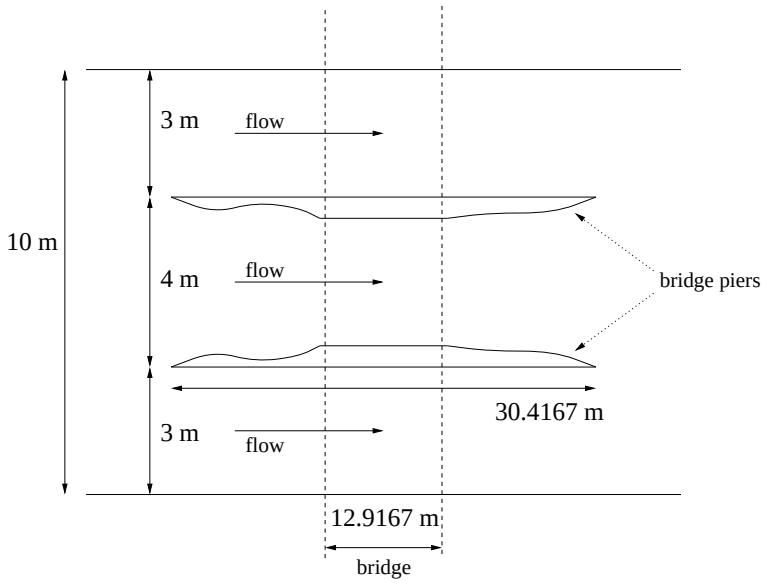


Figure 5.6.2. Channel Configuration for Bridge Pier.

For the outer two reaches, the bridge piers are straight walls parallel to the channel sidewalls. Therefore, in these two regions, the discharge rates do not change, and the flow is almost uniform. Only the flow between the piers is dramatically altered. The characteristics of the channel and inflow are listed in Table 5.6.1.

Table 5.6.1. Geometry and Flow Characteristics for Bridge Pier.

| Characteristic | Value |
|---|---|
| Channel Width | 10.0 $m$ |
| Bed Slope | 0.02 |
| Manning's n | 0.013 |
| Number of Rows | 25 |
| Number of Columns | 135 |
| Maximum Width of Piers | 0.315 m |
| Length of Piers | 30.41667 m |
| Width of Bridge | 12.91667 m |
| Gravity | 9.817 $m/sec^2$ |
| Inflow Depth | 1.50326 $m$ |
| Inflow Velocity | 12.6392 $m/sec$ |
| Inflow Froude Number | 3.29013 |
| Discharge Q | 190.000 $m^3/sec$ |

The primary design goal is to generate uniform flow under the bridge between the two piers, while a secondary design concern is the flow downstream of the piers. Thus, the objective function consists of the sum of the non-uniformity under the bridge and the non-uniformity after the bridge piers. This function can be expressed as

$$F(\vec{\beta}) = \sum_{\vec{x}_k \in \Omega_{F_1}} \left( h_{ave_1}(\vec{\beta}) - h_k(\vec{\beta}) \right)^2 + \sum_{\vec{x}_k \in \Omega_{F_2}} \left( h_{ave_2}(\vec{\beta}) - h_k(\vec{\beta}) \right)^2 \tag{5.6.1}$$

where $h_{ave_1}$ is the average depth under the bridge between the two piers $\Omega_{F_1}$ and $h_{ave_2}$ is the average depth for a region downstream of the bridge piers $\Omega_{F_2}$. For this example, a constraint is placed on the design variables in order to make sure that the bridge piers have positive width. Since the design variables control the width of the piers, placing the constraint that the design variables remain positive is justifiable. Since constrained optimization is a research area beyond the scope of this work, a

simple modification to the optimization algorithm has been made to guarantee that the constraint is satisfied.

Table 5.6.2. Comparison of Design Space Derivatives for Bridge Pier.

| Design Variable | Discrete Sensitivity Analysis | Complex Expansion Method |
|---|---|---|
| 1 | 0.16353328896270 | 0.16353329367119 |
| 2 | -1.2951639359367 | -1.2951639539375 |
| 3 | -2.1287765599801 | -2.1287765752836 |
| 4 | -1.9890777309903 | -1.9890777193054 |
| 5 | -2.3759740481279 | -2.3759740196752 |
| 6 | -2.2237948013474 | -2.2237947999342 |
| 7 | 1.6650382239926 | 1.6650382228846 |
| 8 | 4.0151570077473 | 4.0151570461220 |
| 9 | 4.1614797070326 | 4.1614797029406 |
| 10 | 7.5704068291118 | 7.5704068334812 |
| 11 | 6.5919693269547 | 6.5919693095355 |
| 12 | -10.1790808162469 | -10.179080794322 |

To analyze the accuracy of the design space gradient, the derivatives for the initial set of design variables, which mimics a straight wall, are compared with the exact derivatives generated by the complex Taylor's series expansion method. These design space derivatives are presented in Table 5.6.2 and are highly accurate, agreeing with the exact derivatives to eight or more significant digits. The termination criterion is based on the relative change of the objective function value, so that the design optimization process terminates when this change is less than $10^{-6}$. Thus, after 17 design iterations, the process terminates. The optimization history for the bridge piers example is plotted in Figure 5.6.3. A large number of design iterations is probably required because of the use of an inefficient constrained optimization modification.

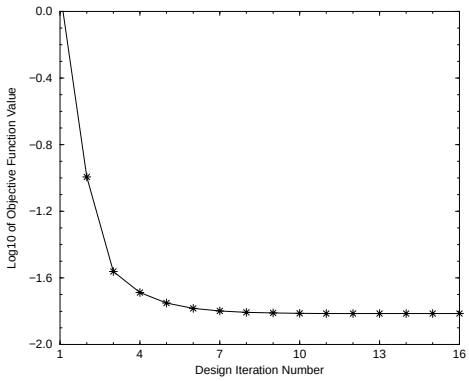


Figure 5.6.3. Optimization History for Bridge Pier Example.

The final shape of the bridge piers and the depth of flow through this design are plotted in Figure 5.6.4. The curved wall contraction pattern is similar to the final curve for the curved wall contraction example in Section 5.3, and the curved wall expansion is similar to the expansion curve in Section 5.4. The flow depths show the same type of undulations as seen in the curved wall contractions and expansions, but the depth under the bridge is almost perfectly level, as is the depth after the contraction. The depth of flow between the pier and the channel wall is relatively undisturbed, as expected.

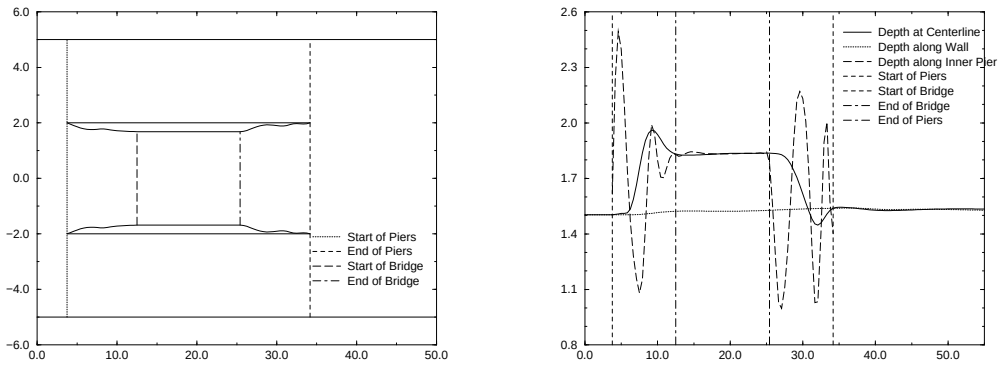


Figure 5.6.4. Shape and Water Surface Profiles for Final Design of Bridge Pier.

For this example, the two design concerns are to generate uniform flow under the bridge between the piers and uniform flow downstream of the piers. Having six design variables control the contraction curve before the bridge and six design variables control the expansion curve after the bridge, these design goals are achieved quite successfully, terminating after 17 design iterations. As seen in the optimization history, most of the design improvement is achieved within five or six iterations. Hence, the design optimization process has efficiently located the region in design space that contains the highly acceptable shapes for the bridge piers that generate uniform flow in the desired locations.